



# X-ray fluorescence mapping of mercury on suspended mineral particles and diatoms in a contaminated freshwater system

B. Gu<sup>1</sup>, B. Mishra<sup>2</sup>, C. Miller<sup>1</sup>, W. Wang<sup>1</sup>, B. Lai<sup>3</sup>, S. C. Brooks<sup>1</sup>, K. M. Kemner<sup>2</sup>, and L. Liang<sup>1</sup>

<sup>1</sup>Environmental Sciences Division, Oak Ridge National Laboratory, Oak Ridge, TN 37831, USA

<sup>2</sup>Biosciences Division, Argonne National Laboratory, Argonne, IL 60439, USA

<sup>3</sup>X-ray Science Division, Argonne National Laboratory, Argonne, IL 60439, USA

Correspondence to: B. Gu (gub1@ornl.gov)

Received: 3 March 2014 – Published in Biogeosciences Discuss.: 23 May 2014

Revised: 18 August 2014 – Accepted: 3 September 2014 – Published: 30 September 2014

**Abstract.** Mercury (Hg) bioavailability and geochemical cycling is affected by its partitioning between the aqueous and particulate phases. We applied a synchrotron-based X-ray fluorescence (XRF) microprobe to visualize and quantify directly the spatial localization of Hg and its correlations with other elements of interest on suspended particles from a Hg-contaminated freshwater system. Up to  $175 \mu\text{g g}^{-1}$  Hg is found on suspended particles, but less than 0.01 % is in the form of methylmercury. Mercury is heterogeneously distributed among phytoplankton (e.g., diatoms) and mineral particles that are rich in iron oxides and natural organic matter (NOM). The diatom-bound Hg is mostly found on outer surfaces of the cells, suggesting passive sorption of Hg on diatoms. Our results indicate that localized sorption of Hg onto suspended particles, including diatoms and NOM-coated oxide minerals, may play an important role in affecting the partitioning, reactivity, and biogeochemical cycling of Hg in natural aquatic environments.

## 1 Introduction

Mercury (Hg) is a global pollutant. Certain anaerobic bacteria can transform inorganic Hg into neurotoxic monomethylmercury (MeHg) (Hu et al., 2013b; Parks et al., 2013), which is the most worrisome because MeHg can be readily bioaccumulated in food chains to levels harmful to both humans and wildlife (Barkay and Wagner-Dobler, 2005; Mason et al., 1995; Watras and Bloom, 1992). Suspended particulates including both colloidal minerals and phytoplankton (such as diatoms) are important carriers of Hg and

MeHg in freshwater ecosystems (Adams et al., 2009; Balogh et al., 2008; Choe et al., 2003; Pickhardt and Fisher, 2007; Plourde et al., 1997). Nearly 90 % of the total Hg in water has been reported to be suspended particle bound (Balogh et al., 2008; Choe et al., 2003; Pickhardt and Fisher, 2007), but the exact localization and chemical characteristics of particulate Hg have been poorly studied to date. Similarly in the contaminated East Fork Poplar Creek (EFPC) at the US Department of Energy's (DOE) Y-12 National Security Complex (NSC) in Oak Ridge, Tennessee, about 75–95 % of the Hg is associated with suspended particles (Brooks and Southworth, 2011) (Supplement Fig S1), although the range of particle-bound Hg varies with season, flow conditions, and the distance from the contamination source. In freshwater lakes and stream systems, studies have also shown that Hg mainly associates with particulate natural organic matter (NOM) and iron and aluminum oxyhydroxides (Adams et al., 2009; Quemerais et al., 1998), resulting in elevated Hg concentrations on these particles since Hg sorption on phyllosilicate minerals is relatively low (Hintelmann and Harris, 2004; Senevirathna et al., 2011). The association of Hg with riverine particles is usually attributed to passive adsorption, and both abiotic and biological processes are important for this process (Mason et al., 1996; Pickhardt and Fisher, 2007). However, the accumulation of MeHg by phytoplankton is attributed primarily to an active uptake process, resulting in the biomagnification of Hg in aquatic food chains from phytoplankton to fish (Barkay and Wagner-Dobler, 2005; Mason et al., 1995; Watras and Bloom, 1992). For example, in a study of the bioaccumulation of inorganic Hg and MeHg by freshwater phytoplankton, Pickhardt and Fisher (2007) found that the

volume concentration factors (VCFs) for the inorganic Hg on phytoplankton ranged from 0.5 to  $5 \times 10^4$ , whereas VCFs for MeHg were about 20–30 times higher, ranging from 1.3 to  $15 \times 10^5$ . Additionally, these authors showed that about 84 to 91 % of inorganic Hg is associated with cell surfaces (Pickhardt and Fisher, 2007). Similarly, Mason et al. (1996) reported that Hg(II) is principally bound to phytoplankton membranes, whereas MeHg is largely accumulated inside the cell, in the cytoplasm.

Hg association with phytoplankton cell membranes has been traditionally determined by the difference between total Hg in the whole cell and that in the cytoplasmic fraction of lysed cells that are obtained following mechanical grinding or sonification and separation (Mason et al., 1996; Pickhardt and Fisher, 2007). This is partly because the very low Hg concentrations in natural water that result in a relatively low level of Hg on cell surfaces; thus to assay the low cell-surface-bound Hg, highly sensitive techniques such as cold-vapor atomic absorption or fluorescence spectroscopy are needed for quantification. However, complications may occur in such assays due to possible interactions between cell wall-associated Hg and cytoplasmic Hg, resulting in re-partitioning (sorption or desorption) of Hg on cell membranes. More importantly, these techniques cannot discern the localization of sorbed Hg in natural samples consisting of both mineral and phytoplankton particles. Whether the sorbed Hg is evenly or heterogeneously distributed on the particles is unknown. Techniques such as X-ray fluorescence (XRF) microprobes could potentially provide direct and accurate localization and characterization of Hg on suspended particles of mixed mineral or organic origins. Such techniques have been used to map two-dimensional (2-D) and 3-D elemental distributions over length scales from sub-micrometers to tens of millimeters, covering microbial cells, soil, and plant roots (Bernaus et al., 2006; Blute et al., 2004; De Jonge et al., 2010; Kemner et al., 2004; Terzano et al., 2010). The spatial resolution and elemental sensitivity of X-ray fluorescence extend below 100 nm and are able to detect, for example, arsenic at  $30\text{--}1200 \mu\text{g g}^{-1}$  on cattail root plaques (Blute et al., 2004) and as low as  $1 \mu\text{g g}^{-1}$  within a single bacterial cell (Kemner et al., 2004). Furthermore, the technique allows simultaneous detection of multiple elements and can provide a powerful tool to map their spatial distribution and correlations.

In this study, we used XRF microprobes to examine Hg distributions and its correlations with multiple elements of interest on both diatoms and mineral particles. To our knowledge, this is the first time XRF microprobes have been used to map the localization of Hg on suspended particles in a contaminated freshwater ecosystem. We hypothesized that localized sorption of Hg occur on suspended particles with different binding affinities and that particulate organic matter or NOM-coated iron oxyhydroxides sorb more Hg than those of phyllosilicate minerals. Complementary techniques including inductively coupled plasma mass spectrometry (ICP-

MS), Fourier transform infrared (FTIR), scanning electron microscopy (SEM) and elemental mapping were used to determine the bulk loading of Hg and MeHg on particles and the association of NOM with minerals. Results of this study are expected to have important implications in determining Hg partitioning, geochemical cycling, and bioavailability in the natural aquatic environment.

### 1.1 Materials and methods

Suspended particles from the contaminated EFPC water in Oak Ridge, Tennessee, were obtained during two sampling campaigns along a 2.5 km stretch from its headwater within the Y-12 NSC (Brooks and Southworth, 2011; Miller et al., 2009). Past industrial operations and processes at site resulted in the release of more than 200 metric tons of Hg into the water and sediments (Barnett et al., 1997; Brooks and Southworth, 2011; Miller et al., 2009). The total Hg concentration in the headwater remains high at  $\sim 1000 \text{ ng L}^{-1}$ . The water in EFPC is a Ca–Mg– $\text{HCO}_3^-$  type composition with a slightly alkaline pH ranging from 7.4 to 8.0. Creek water was first collected in plastic bottles and transported to the laboratory in a cooler on ice. During the first sampling in early spring, suspended solids were collected at three locations including EFK25.9, EFK25.1, and EFK23.5, which are approximately 0.1, 0.9, and 2.5 km, respectively, from the headwater, with a total Hg concentration in water decreasing from  $\sim 1000$  to  $200 \text{ ng L}^{-1}$  (Brooks and Southworth, 2011; Miller et al., 2009). The total particle concentration in water was determined by collecting and weighing the particulate matter on a  $0.2 \mu\text{m}$  membrane filter after drying. Suspended particles were separated into two different size fractions (between 0.2 and  $3 \mu\text{m}$ , and greater than  $3 \mu\text{m}$ ) using membrane filtration. The  $> 3 \mu\text{m}$  fraction contained mostly diatoms and large mineral particles or aggregates, whereas the  $< 3 \mu\text{m}$  fraction consisted mostly of mineral particles. During the second sampling in late fall, samples were collected only at the EFK23.5 location, and particles were separated by centrifugation at 4000 rpm in 250 mL bottles and then resuspended in a small amount of the creek water in 3 mL vials. They were stored in a freezer ( $-20^\circ\text{C}$ ) until use. Total Hg and MeHg concentrations on suspended solids were analyzed using established procedures (described below).

Size and morphological properties of suspended particles were subsequently evaluated with a Zeiss Merlin scanning electron microscopy (SEM) operated at 3 kV. Particulate samples were mounted by allowing a small drop of the suspension to evaporate either on a silicon nitride membrane or a copper transmission electron microscopy (TEM) grid with carbon-Formvar coatings. Energy-dispersive X-ray (EDX) spectra of selected diatoms and mineral particles were recorded at 20 kV with a Quantax microanalysis system (Bruker-AXS Microanalysis GmbH, Berlin, Germany), and electron backscattering elemental analysis was also performed with the same system. Fourier transform infrared

(FTIR) spectroscopy of selected samples in the size fraction between 0.2 and 3  $\mu\text{m}$  was performed with a Nicolet Magna 760 spectrophotometer (Nicolet Instrument Corp.). A small droplet of particulate samples was placed onto a ZnSe window and allowed to dry before the window was inserted in the IR beam for analysis. The spectral resolution was 4  $\text{cm}^{-1}$ .

Localization and 2-D XRF elemental maps were determined on two sets of selected diatom and particulate samples, with the first set (collected in the spring at EFK23.5) used as is and the other collected in the late fall at the same location but amended with Hg(II) (as  $\text{HgCl}_2$ , 2.9  $\mu\text{M}$ ) at pH 7.8 (same as in the creek water) for comparisons. The final sorbed Hg concentration was 617  $\mu\text{g g}^{-1}$  dry wt, which is about 3–10 times higher than that observed in natural EFPC water. The XRF analysis was performed at beamline 2ID-D at the Advanced Photon Source at Argonne National Laboratory, United States (Cai et al., 2000; Kemner et al., 2004). Fresnel zone plates are used as focusing optics in hard X-ray microprobes at energies typically between 6 and 30 keV. Highly focused X-rays are used to quantify and map trace elements in heterogeneous materials with low detection limits at the sub-micron spatial resolution. The microprobe excites the specimen with an intense X-ray beam and measures the energies and intensities of emitted X-rays, allowing quantification of the concentration of elements in a heterogeneous sample matrix.

The X-ray probe energy was set to 12 300 eV (16 eV above Hg  $L_{\text{III}}$  edge) and the sample chamber was flushed with He for the X-ray measurement, as described previously (Glasauer et al., 2007). The size of the beam at the focal point was 150 nm (V)  $\times$  200 nm (H) at FWHM (full width at half maximum), determined by scans with a Cr knife edge. Step size for the final raster scans of the diatoms and particulates were 100 nm. Incident and transmitted beam intensities were monitored with air-filled ionization detectors. XRF signals from the samples were detected by a single-element Ge detector placed perpendicular to the incident beam direction in the plane of polarization.

The XRF concentration maps of elements from Si to Hg were obtained, although only those of Si, Ca, S, Fe, Mn, Zn, Hg, P, and Cl were presented because of their relatively high concentrations. The XRF peaks of interest were fitted by modified Gaussian profiles to separate the XRF signal from background in the spectrum. Quantitative elemental analysis in several regions of each sample was done by averaging the multi-channel analyzer (MCA) spectra collected within these regions, subtracting the averaged MCA spectra for regions outside the diatoms or mineral particles (representative of an experimental background signal) and then integrating the counts within each region of interest. The integrated MCA counts were converted to area concentrations of elements in each sample by comparing the XRF intensities between the samples and thin glass film standards 1832 and 1833 (obtained from the National Institute of Standards and Technology – NIST) measured under the same experimental

conditions and normalized to incident X-ray beam intensity (Cai et al., 2000; Kemner et al., 2004). Under given operation conditions, the estimated detection limits were about  $10^{-4}$   $\mu\text{g cm}^{-2}$  for Hg,  $\sim 3 \times 10^{-4}$  to  $2 \times 10^{-3}$   $\mu\text{g cm}^{-2}$  for Mn, Fe, Ni, and Zn, and  $\sim 2$   $\mu\text{g cm}^{-2}$  for Si, P, and Cl (Ortega et al., 2004; Twining et al., 2003). We note however that the detection limit is affected by factors such as the incident energy used to probe the sample, the atomic number of the element, and the sample matrix.

For the determination of bulk total Hg, MeHg, and elemental compositions on particles, the first set of samples were separated into two size fractions of (i) greater than 3  $\mu\text{m}$  and (ii) greater than 0.2  $\mu\text{m}$  but less than 3  $\mu\text{m}$ , with the corresponding membrane filters (Supor and GF/C Glass Fiber). Particles were digested in a 1:1 mixture of concentrated nitric and hydrochloric acids. Bromine monochloride ( $\text{BrCl}$ ) was added to half of the digestion mixture for the determination of total Hg by cold vapor atomic fluorescence spectrometry (CVAFS) (Miller et al., 2009; Zheng et al., 2012). Briefly, hydroxyammonium hydrochloride ( $\text{NH}_2\text{OHHCl}$ ) was added to the digest to remove free halogens followed by the addition of stannous chloride ( $\text{SnCl}_2$ ) to reduce Hg(II) to gaseous Hg(0), which was trapped onto a gold trap and subsequently thermally desorbed into a  $\text{N}_2$  gas stream and analyzed by CVAFS (Gu et al., 2011; Hu et al., 2013b). The remaining digest was diluted and used to determine the total elemental compositions, including major ions of Fe, Al, Mn, Ca, Mg, and Zn, by inductively coupled plasma-mass spectrometry (ICP-MS, Perkin-Elmer). MeHg concentrations were determined based on a modified US EPA Method 1630 involving the distillation of samples followed by ethylation, gas chromatographic separation, and detection by ICP-MS (Hu et al., 2013b; Parks et al., 2013).

## 2 Results and discussion

Total suspended particles ( $> 0.2$   $\mu\text{m}$ ) collected from the EFPC ranged from about 3  $\text{mg L}^{-1}$  to 5.5  $\text{mg L}^{-1}$  under steady flow conditions. These particles comprised a mixture of diatoms (usually greater than 5  $\mu\text{m}$ ) and mineral particulates (Fig. 1a) and their dominant elemental compositions were Si, Al, O, and C as determined by EDX analysis (Fig. 1b) (Note that Cu was an artifact resulting from the use of copper grid sample holders). Using acid digestion coupled with ICP-MS analysis, we determined the dominant metal ions in samples were Fe, Al, Mg, Mn, and Zn (Fig. 1c), with the smaller size fraction (between 0.2 and 3  $\mu\text{m}$ ) showing slightly higher amounts of Fe and Al on a dry weight basis. The presence of zinc is consistent with the industrial effluents entering the headwaters of EFPC. As expected, a large percentage of Hg ( $> 80\%$ ) is associated with particles, and the highest Hg concentration observed was  $\sim 175$   $\mu\text{g g}^{-1}$  dry weight (Fig. 1d). The smaller size fractions (between 0.2 and 3  $\mu\text{m}$ ) also showed slightly

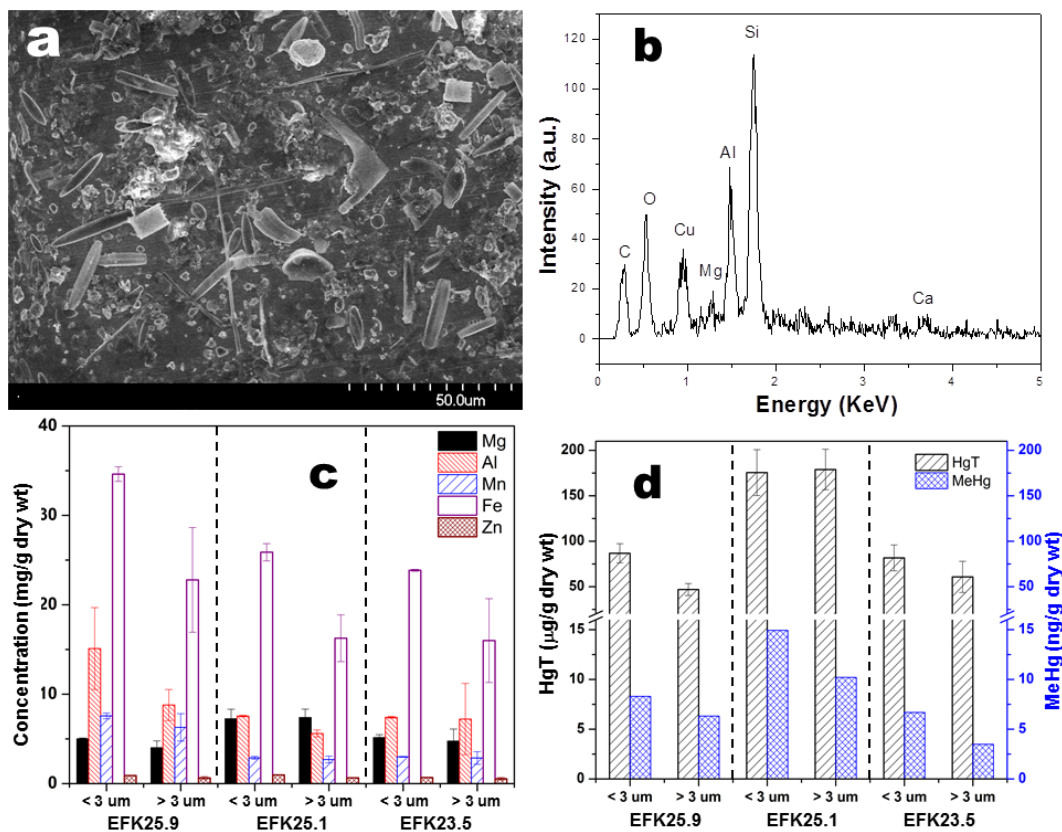


**Figure 1.** (a) SEM image of suspended particulates containing both diatoms and mineral particles from EFPC in Oak Ridge, Tennessee; (b) energy dispersive X-ray (EDX) analysis of particulates in (a), showing the dominant elemental composition of Si, Al, O, and C (note: the Cu signal is from the use of copper grid sample holders); (c) bulk analysis of major cations on EFPC particles collected from three locations (EFK25.9, EFK25.1, and EFK23.5) and two size fractions by ICP-MS following digestion in 1 : 1 concentrated HCl : HNO<sub>3</sub>; (d) distribution of total Hg (HgT) and MeHg associated with EFPC particles of two different size fractions.

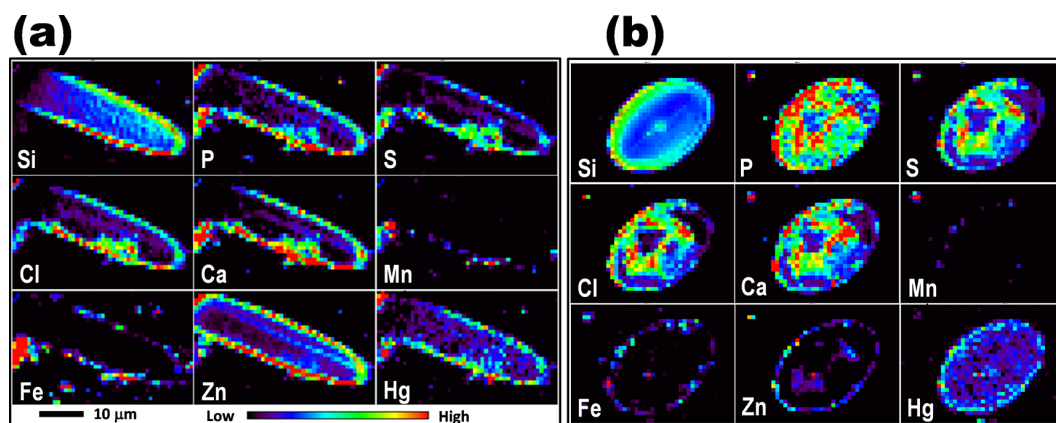
higher levels of sorbed total Hg and MeHg than those of the larger size fraction (> 3 μm), except samples collected 0.9 km downstream of the headwater (EFK25.1). The MeHg concentrations in these samples were generally low or below the detection limit (Fig. 1d) and represents only a tiny fraction (< 0.01 %) of the total Hg associated with particles.

Despite Hg concentrations lower than typically amenable to X-ray techniques, we were able to detect and map Hg on surfaces of these particles by XRF on individual diatoms and mineral particles (Figs. 2 and 3). Four individual diatoms with different morphological properties and Hg-loadings (with or without Hg additions) were studied along with mineral particulate clusters (Fig. 4). We analyzed Hg on diatoms and mineral particles by conducting XRF microscopy measurements and signal collection both above and below the Hg L<sub>III</sub> edge to confirm that the observed Hg signal is not an artifact due to spectral leakage from other elements. Hg appears to be co-localized with Fe, Mn, S, Zn, P, Cl, and Ca in most cases, but not with Si on both diatoms and mineral particles (Fig. 3, details are shown in the individual sub-figures of the lower left in 3a and the upper left

in 3b). The correlations between Hg and P, Cl, S, and Ca are consistent with the association of Hg with biomass either as cellular components or preferred ligands (in the case of S) (Glasauer et al., 2007). This is also shown in the electron backscattering analysis of these elements (Supplement Fig. S2). Other elements were not shown due to their relatively low concentrations or insensitivity to XRF microscopy. Provided in Table 1 is the average elemental composition on the entire diatom and selected mineral particles determined with XRF in Figs. 2–4. On a micron scale (at 100 nm resolution), quantification of Hg concentrations on diatoms and minerals revealed highly heterogeneous distribution, particularly on mineral particles with localized areas of high Hg concentrations. For diatoms, with the exception of locations in the lower part of the diatoms in Fig. 3, Hg is predominantly associated with cell walls or outer membranes. This observation suggests that surface adsorption of Hg(II) is the main process for Hg uptake by diatoms, since more than 99 % of the Hg in EFPC water is in the form of inorganic Hg(II) (Fig. 1d) (Brooks and Southworth, 2011). It agrees with previous studies, which showed that passive adsorption

**Table 1.** The average elemental compositions ( $\mu\text{g cm}^{-2}$ ) on the entire diatom and selected mineral particles determined by XRF in Figs. 2–4.

Elements	Fig. 2a diatom	Fig. 2b diatom	Fig. 3a diatom	Fig. 3b diatom	Fig. 3a mineral (lower left)	Fig. 3b mineral (top left)	Fig. 4a mineral particles
Si	32	34	32.245	24	5.256	6.0	4.8
P	0.506	0.637	0.126	0.168	0.355	0.220	2.112
S	0.508	0.824	0.149	0.217	0.380	0.387	1.968
Cl	0.998	1.559	0.643	0.651	0.662	0.728	1.352
Ca	1.926	2.152	0.900	1.060	2.138	2.040	3.9
Mn	0.145	0.0569	0.098	0.315	1.560	0.991	1.206
Fe	0.479	0.388	0.800	2.923	9.243	5.434	12.591
Zn	0.220	0.0588	0.190	0.799	0.259	0.147	0.29
Hg	0.006	0.005	0.032	0.092	0.154	0.142	0.138

**Figure 2.** Direct X-ray microprobe fluorescence imaging and elemental analysis of two individual diatoms collected from a Hg-contaminated EFPC creek (EFK23.5) without any treatment. Only selected elements of Hg, Zn, Fe, Mn, Ca, Cl, S, P, and Si were presented due to their relatively high concentrations. The average total Hg content is about  $70 \mu\text{g g}^{-1}$  particles (dry wt).

is the principal mechanism for the membrane-bound Hg on diatoms or phytoplankton since both living and heat-killed cells have similar VCFs for inorganic Hg (Mason et al., 1996; Pickhardt and Fisher, 2007; Watras and Bloom, 1992). The result is also similar to the adsorption of such metal ions as  $\text{Zn}^{2+}$ , which is predominately sorbed onto diatom membranes, rather than Si frustule (Gelabert et al., 2007), and thus explains the co-localization of Hg and Zn since both of them are soft metals. As for MeHg, the VCFs were 1.5–5 times higher in living cells than dead, thus an active uptake by phytoplankton cells has been suggested to be the main mechanism (Pickhardt and Fisher, 2007).

The elevated concentrations of Hg noted on the diatoms in Fig. 3 likely result from mineral particulates such as iron oxides laying on or attached to cells, as evidenced by elevated concentrations of Fe, S, Ca, and Mn in those areas in the image. In general, when normalized to the surface area, average Hg loadings on the mineral particles are higher than the average Hg loadings on the entire diatom (Table 1). Additional analyses of several selected mineral particles (Fig. 4a) indicate a highly heterogeneous distribution of Hg. On many

particles (Fig. 4a, upper two-thirds of the image) Hg was not detected, whereas on others (lower center region), up to about  $0.14 \mu\text{g cm}^{-2}$  Hg was measured (Table 1). Similar to observations on diatoms, Hg on mineral particles was co-localized with Fe, Mn, S, and Zn, but not with Si. These correlations are not completely surprising and can be attributed to the presence of iron and manganese oxide minerals and the associated NOM coatings and microbial biomass, which are known to sorb Hg strongly (Dong et al., 2011; Hu et al., 2013a, 2013b).

Significant sorption of NOM on iron and manganese oxide minerals is expected because of their strong binding affinities, as shown in previous studies (Fu and Quan, 2006; Gu et al., 1994; 1995; Parfitt et al., 1977; Schwertmann et al., 1986). A strong association between NOM and naturally occurring iron or manganese oxyhydroxides is commonly observed in water (Balogh et al., 2008; Gu et al., 1994; Hintelmann and Harris, 2004; Quemerais et al., 1998). The dissolved organic matter concentration in EFPC water is  $\sim 3 \text{ mg L}^{-1}$  (Dong et al., 2010; Miller et al., 2009). Using the electron backscattering elemental analysis we can

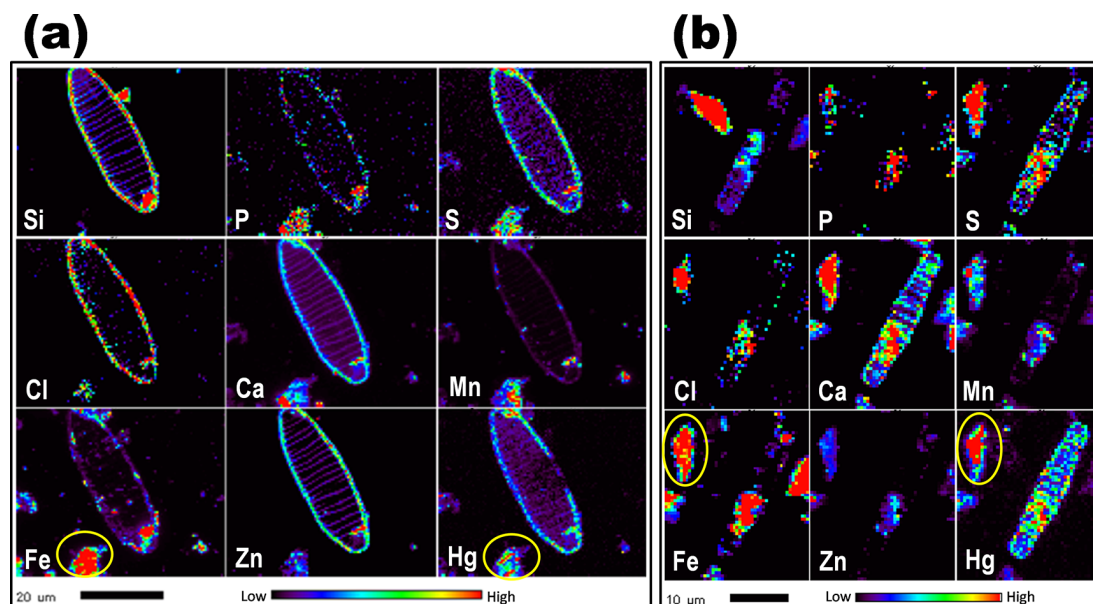


**Figure 3.** X-ray microprobe fluorescence imaging and elemental analysis of two individual diatoms and mineral particles with different morphologies collected from a Hg-contaminated EFPC creek (EFK23.5). Both samples were spiked with Hg to a final sorbed Hg concentration of  $617 \mu\text{g g}^{-1}$  (dry wt) on average (see text for additional details). Iron-rich mineral particles can be seen at the lower left of the image (a) and upper left of the image (b) (yellow circles).

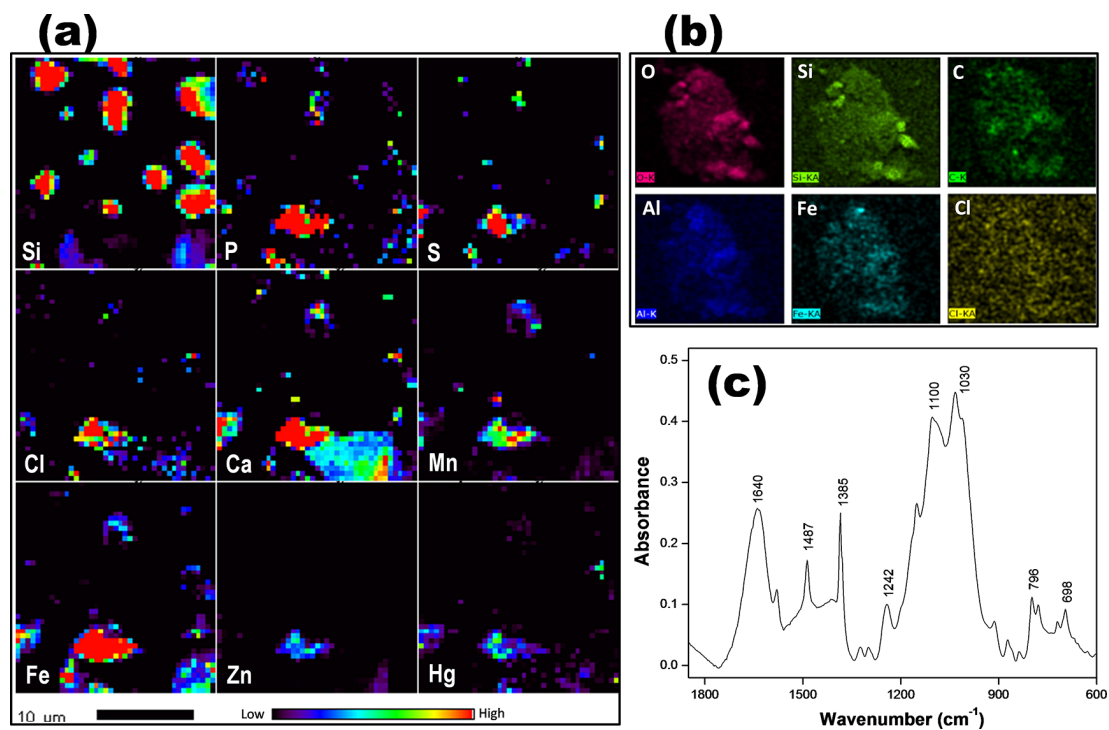


**Figure 4.** Experiments used to support the hypothesis that organic matter (carbon) is associated with iron oxide minerals and acts as a bridge for Hg sorption. (a) X-ray microprobe fluorescence imaging and elemental analysis (e.g., Hg, Fe, etc.) of selected mineral particles (from EFK23.5) spiked with Hg at  $617 \mu\text{g g}^{-1}$  (dry wt); (b) scanning electron microscope (SEM) backscattering elemental analysis of a selected cluster of mineral particles showing the association between carbon and Fe, and (c) FTIR spectroscopic analysis of natural organic matter associated with mineral particles.

clearly distinguish the organic carbon (C) coating on mineral particles ( $<3\ \mu\text{m}$ ) (Fig. 4b) and, more importantly, the distribution of C in the image appears well correlated with those of Fe, Al, and O. Additionally, the FTIR spectrum of mineral particles showed strong absorbance bands in the region between  $1000$  and  $1700\ \text{cm}^{-1}$  (Fig. 4c), indicating the presence of organic matter with carboxylic and phenolic carbon moieties (at  $\sim 1640\ \text{cm}^{-1}$ ) (Fu and Quan, 2006; Gu et al., 1994; 1995; Tejedor-Tejedor and Anderson, 1990). The broad band between  $900\ \text{cm}^{-1}$  and  $1200\ \text{cm}^{-1}$  also suggests the presence of organic matter such as polysaccharide C–O functional groups that are likely associated with minerals (Fu and Quan, 2006; Gu et al., 1994; 1995; Parfitt et al., 1977). The absorbance peaks at about  $1030$ ,  $800$ ,  $750$ , and  $700\ \text{cm}^{-1}$  could be attributed to the presence of minerals such as lepidocrocite and goethite (Parfitt et al., 1992; Schwertmann and Wolska, 1990).

These observations and analyses (Fig. 4b,c) suggest that NOM-coated iron-oxyhydroxide minerals may serve as strong sorption sites for Hg through the formation of Hg–NOM complexes. In other words, these organic materials may have acted as a bridging agent by forming the Hg–(S–NOM–O)–Fe oxide ternary complexes because the complexation between iron oxides and NOM involves primarily the carboxyl and hydroxyl functional groups (Fu and Quan, 2006; Gu et al., 1994, 1995; Tejedor-Tejedor et al., 1992), whereas Hg binding with NOM occurs through reduced sulfur functional groups on NOM (Dong et al., 2011; Gu et al., 2011; Miller et al., 2009; Nagy et al., 2011; Skyllberg et al., 2006). As a result, it led to greatly increased Hg loadings on these particles (Table 1).

### 3 Conclusions

XRF microprobe imaging is shown to provide a useful tool for directly visualizing and quantifying the localization of Hg and its correlations to elemental distributions on suspended particles of both living organisms (e.g., diatoms) and inorganic minerals. Relatively high levels of localized Hg on particles (e.g.,  $>50\ \mu\text{g g}^{-1}$ ) may be needed for XRF analysis, and this level of Hg could be found in contaminated water bodies such as the EFPC water with dissolved Hg concentrations of more than  $100\ \text{ng L}^{-1}$  and the San Francisco Bay delta waters (Pickhardt and Fisher, 2007). The technique is particularly useful for identifying the presence or absence of certain minerals and particles such as cinnabar or metacinnabar based on the clustering of Hg with S or other elements (Bernaus et al., 2006; Terzano et al., 2010). It is important to realize the ubiquitous presence of NOM and its association with iron oxyhydroxides, which can enhance Hg uptake by suspended particles in freshwater ecosystems. These organic materials sorb onto Fe and Al oxide surfaces via carboxyl or hydroxyl functional groups, whereas sulfhydryl functional groups in NOM form complexes with

Hg(II). Such an intimate association between Hg and NOM and suspended particles could potentially control the partitioning and reactivity of Hg, and may thus have important implications in determining the geochemical cycling and bioavailability of Hg in natural aquatic environments.

**The Supplement related to this article is available online at doi:10.5194/bg-11-5259-2014-supplement.**

*Acknowledgements.* This research was sponsored by the Office of Biological and Environmental Research (BER), Office of Science, US Department of Energy (DOE) as part of the Mercury Science Focus Area Program at ORNL, which is managed by UT-Battelle LLC for the DOE under contract DE-AC05-00OR22725. Partial support for B. Mishra and K. M. Kemner was provided by the Subsurface Science Focus Area program at Argonne National Laboratory (ANL) which is supported by BER under contract DE-AC02-06CH11357. Use of the Advanced Photon Source, an Office of Science User Facility at ANL, was supported by DOE under contract DE-AC02-06CH11357.

Edited by: E. Pendall

### References

- Adams, R. M., Twiss, M. R., and Driscoll, C. T.: Patterns of mercury accumulation among seston in lakes of the Adirondack Mountains, New York, *Environ. Sci. Technol.*, 43, 4836–4842, 2009.
- Balogh, S. J., Swain, E. B., and Nollet, Y. H.: Characteristics of mercury speciation in Minnesota rivers and streams, *Environ. Pollut.*, 154, 3–11, 2008.
- Barkay, T. and Wagner-Dobler, I.: Microbial transformations of mercury: potentials, challenges, and achievements in controlling mercury toxicity in the environment, *Adv. Appl. Microbiol.*, 57, 1–52, 2005.
- Barnett, M. O., Harris, L. A., Turner, R. R., Stevenson, R. J., Henson, T. J., Melton, R. C., and Hoffman, D. P.: Formation of mercuric sulfide in soil, *Environ. Sci. Technol.*, 31, 3037–3043, 1997.
- Bernaus, A., Gaona, X., van Ree, D., and Valiente, M.: Determination of mercury in polluted soils surrounding a chlor-alkali plant – direct speciation by X-ray absorption spectroscopy techniques and preliminary geochemical characterisation of the area, *Anal. Chim. Acta*, 565, 73–80, 2006.
- Blute, N. K., Brabander, D. J., Hemond, H. F., Sutton, S. R., Newville, M. G., and Rivers, M. L.: Arsenic sequestration by ferric iron plaque on cattail roots, *Environ. Sci. Technol.*, 38, 6074–6077, 2004.
- Brooks, S. C. and Southworth, G. R.: History of mercury use and environmental contamination at the Oak Ridge Y-12 Plant, *Environ. Pollut.*, 159, 219–228, 2011.
- Cai, Z., Lai, B., Yun, W., Ilinski, P. P., Legnini, D. G., Maser, J., and Rodrigues, W.: Hard X-ray scanning microprobe for fluorescence imaging and microdiffraction at the advanced photon source, in:

- X-Ray Microscopy, edited by: Meyer-Ilse, W., Warwick, T., and Attwood, D., Proceedings of the 6th International Conference, American Institute of Physics, New York, 2000.
- Choe, K. Y., Gill, G. A., and Lehman, R.: Distribution of particulate, colloidal, and dissolved mercury in San Francisco Bay estuary. 1. Total mercury, *Limnol. Oceanogr.*, 48, 1535–1546, 2003.
- de Jonge, M. D., Holzner, C., Baines, S. B., Twining, B. S., Ignatyev, K., Diaz, J., Howard, D. L., Legnini, D., Miceli, A., McNulty, I., Jacobsen, C. J., and Vogt, S.: Quantitative 3-D elemental microtomography of *Cyclotella meneghiniana* at 400-nm resolution, *P. Natl. Acad. Sci. USA*, 107, 15676–15680, 2010.
- Dong, W., Liang, L., Brooks, S. C., Southworth, G., and Gu, B.: Roles of dissolved organic matter in the speciation of mercury and methylmercury in a contaminated ecosystem in Oak Ridge, Tennessee, *Environ. Chem.*, 7, 94–102, 2010.
- Dong, W., Bian, Y., Liang, L., and Gu, B.: Binding constants of mercury and dissolved organic matter determined by a modified ion exchange technique, *Environ. Sci. Technol.*, 45, 3576–3583, 2011.
- Fu, H. B. and Quan, X.: Complexes of fulvic acid on the surface of hematite, goethite, and akaganeite: FTIR observation, *Chemosphere*, 63, 403–410, 2006.
- Gelabert, A., Pokrovsky, O. S., Schott, J., Boudou, A., and Feurtet-Mazel, A.: Cadmium and lead interaction with diatom surfaces: A combined thermodynamic and kinetic approach, *Geochim. Cosmochim. Ac.*, 71, 3698–3716, 2007.
- Glasauer, S., Langley, S., Boyanov, A., Lai, B., Kemner, K., and Beveridge, T. J.: Mixed-valence cytoplasmic iron granules are linked to anaerobic respiration, *Appl. Environ. Microbiol.*, 73, 993–996, 2007.
- Gu, B., Schmitt, J., Chen, Z., Liang, L., and McCarthy, J. F.: Adsorption and desorption of natural organic matter on iron oxide: mechanisms and models, *Environ. Sci. Technol.*, 28, 38–46, 1994.
- Gu, B., Schmitt, J., Chen, Z., Liang, L., and McCarthy, J. F.: Adsorption and desorption of different organic matter fractions on iron oxide, *Geochim. Cosmochim. Ac.*, 59, 219–229, 1995.
- Gu, B., Bian, Y., Miller, C. L., Dong, W., Jiang, X., and Liang, L.: Mercury reduction and complexation by natural organic matter in anoxic environments, *P. Natl. Acad. Sci. USA*, 108, 1479–1483, 2011.
- Hintelmann, H. and Harris, R.: Application of multiple stable mercury isotopes to determine the adsorption and desorption dynamics of Hg(II) and MeHg to sediments, *Mar. Chem.*, 90, 165–173, 2004.
- Hu, H., Lin, H., Zheng, W., Rao, B., Feng, X. B., Liang, L., Elias, D. A., and Gu, B.: Mercury reduction and cell-surface adsorption by *Geobacter sulfurreducens* PCA, *Environ. Sci. Technol.*, 47, 10922–10930, 2013a.
- Hu, H., Lin, H., Zheng, W., Tomanicek, S. J., Johs, A., Feng, X. B., Elias, D. A., Liang, L., and Gu, B.: Oxidation and methylation of dissolved elemental mercury by anaerobic bacteria, *Nat. Geosci.*, 6, 751–754, 2013b.
- Kemner, K. M., Kelly, S. D., Lai, B., Maser, J., O'Loughlin, E. J., Sholto-Douglas, D., Cai, Z. H., Schneegurt, M. A., Kulpa, C. F., and Nealson, K. H.: Elemental and redox analysis of single bacterial cells by X-ray microbeam analysis, *Science*, 306, 686–687, 2004.
- Mason, R. P., Reinfelder, J. R., and Morel, F. M. M.: Bioaccumulation of Mercury and Methylmercury, *Water Air. Soil. Poll.*, 80, 915–921, 1995.
- Mason, R. P., Reinfelder, J. R., and Morel, F. M. M.: Uptake, toxicity, and trophic transfer of mercury in a coastal diatom, *Environ. Sci. Technol.*, 30, 1835–1845, 1996.
- Miller, C., Southworth, G., Brooks, S. C., Liang, L., and Gu, B.: Kinetic controls on the complexation between mercury and dissolved organic matter in a contaminated environment, *Environ. Sci. Technol.*, 43, 8548–8553, 2009.
- Nagy, K. L., Manceau, A., Gasper, J. D., Ryan, J. N., and Aiken, G. R.: Metallothionein-like multinuclear clusters of mercury(II) and sulfur in peat, *Environ. Sci. Technol.*, 45, 7298–7306, 2011.
- Ortega, R., Bohic, S., Tucoulou, R., Somogyi, A., and Deves, G.: Microchemical element imaging of yeast and human cells using synchrotron X-ray microprobe with Kirkpatrick-Baez optics, *Anal. Chem.*, 76, 309–314, 2004.
- Parfitt, R. L., Fraser, A. R., and Farmer, V. C.: Adsorption on hydrous oxides. III. fulvic acid and humic acid on goethite, gibbsite and imogolite, *J. Soil Sci.*, 28, 289–296, 1977.
- Parfitt, R. L., Vandergaast, S. J., and Childs, C. W.: A structural model for natural siliceous ferrihydrite, *Clay. Clay Miner.*, 40, 675–681, 1992.
- Parks, J. M., Johs, A., Podar, M., Bridou, R., Hurt, R. A., Smith, S. D., Tomanicek, S. J., Qian, Y., Brown, S. D., Brandt, C. C., Palumbo, A. V., Smith, J. C., Wall, J. D., Elias, D. A., and Liang, L.: The genetic basis for bacterial mercury methylation, *Science*, 339, 1332–1335, 2013.
- Pickhardt, P. C. and Fisher, N. S.: Accumulation of inorganic and methylmercury by freshwater phytoplankton in two contrasting water bodies, *Environ. Sci. Technol.*, 41, 125–131, 2007.
- Plourde, Y., Lucotte, M., and Pichet, P.: Contribution of suspended particulate matter and zooplankton to MeHg contamination of the food chain in midnorthern Quebec (Canada) reservoirs, *Can. J. Fish. Aquat. Sci.*, 54, 821–831, 1997.
- Quemerais, B., Cossa, D., Rondeau, B., Pham, T. T., and Fortin, B.: Mercury distribution in relation to iron and manganese in the waters of the St. Lawrence river, *Sci. Total Environ.*, 213, 193–201, 1998.
- Schwertmann, U. and Wolska, E.: The influence of aluminum on iron-oxides. Al-for-Fe substitution in synthetic lepidocrocite, *Clay. Clay Miner.*, 38, 209–212, 1990.
- Schwertmann, U., Kodama, H., and Fischer, W. R.: Mutual interactions between organics and iron oxides, in: *Interactions of Soil Minerals with Natural Organics and Microbes*, SSSA Spec. Pub. 17, Soil Science Society of America, Madison, WI, 1986.
- Senevirathna, W. U., Zhang, H., and Gu, B.: Effect of carboxylic and thiol ligands (oxalate, cysteine) on the kinetics of desorption of Hg(II) from kaolinite, *Water Air Soil Poll.*, 215, 573–584, 2011.
- Skylberg, U., Bloom, P. R., Qian, J., Lin, C. M., and Bleam, W. F.: Complexation of mercury(II) in soil organic matter: EXAFS evidence for linear two-coordination with reduced sulfur groups, *Environ. Sci. Technol.*, 40, 4174–4180, 2006.
- Tejedor-Tejedor, M. I. and Anderson, M. A.: Protonation of phosphate on the surface of goethite as studied by Cir-FTIR and electrophoretic mobility, *Langmuir*, 6, 602–611, 1990.



- Tejedor-Tejedor, M. I., Yost, E. C., and Anderson, M. A.: Characterization of benzoic and phenolic complexes at the goethite/aqueous solution interface using cylindrical internal reflection Fourier transform infrared spectroscopy. 2. Bonding structures, *Langmuir*, 8, 525–533, 1992.
- Terzano, R., Santoro, A., Spagnuolo, M., Vekemans, B., Medici, L., Janssens, K., Gottlicher, J., Denecke, M. A., Mangold, S., and Ruggiero, P.: Solving mercury (Hg) speciation in soil samples by synchrotron X-ray microspectroscopic techniques, *Environ. Pollut.*, 158, 2702–2709, 2010.
- Twining, B. S., Baines, S. B., Fisher, N. S., Maser, J., Vogt, S., Jacobsen, C., Tovar-Sanchez, A., and Sanudo-Wilhelmy, S. A.: Quantifying trace elements in individual aquatic protist cells with a synchrotron X-ray fluorescence microprobe, *Anal. Chem.*, 75, 3806–3816, 2003.
- Watras, C. J. and Bloom, N. S.: Mercury and methylmercury in individual zooplankton – implications for bioaccumulation, *Limnol. Oceanogr.*, 37, 1313–1318, 1992.
- Zheng, W., Liang, L., and Gu, B.: Mercury reduction and oxidation by reduced natural organic matter in anoxic environments, *Environ. Sci. Technol.*, 46, 292–299, 2012.